Progress in Scale Modeling, an International Journal

Volume 3 | Issue 1 Article 3

2022

A CFD-based scaling analysis on liquid and paint droplets moving through a weak concurrent airflow stream

Masoud Arabghahestani
Institute of Research for Technology Development (IR4TD), University of Kentucky, mar243@uky.edu

Nelson Akafuah
University of Kentucky, nelson.akafuah@uky.edu

Tianxiang Li
Institute of Research for Technology Development (IR4TD), University of Kentucky, tianxiang.li@uky.edu

Kozo Saito
University of Kentucky, ksaito@uky.edu

A CFD-based scaling analysis on liquid and paint droplets moving through a weak concurrent airflow stream

Category

Research Article

Abstract

We conducted volume of fluids (VOF) multiphase model numerical simulations to obtain the interaction among all the major governing forces identified in our previous paper. Our numerical experiments are intended to assess the droplet generation process and the jetting behavior by providing specific input conditions, offering CFD as a tool to study scaling correlations instead of physical experiments. Water droplets that can represent waterborne paints were generated by piezo-generated sinusoidal waveforms at the inlet of the nozzle. The governing forces included the external piezo-based wave-generation force, the inertial force of droplets, the inertial force of air, the viscose force of air acting on droplet surface, the viscous force of liquid, and surface tension force of droplets. The law approach-based scaling theory was applied to explain the significance of traditional pi-numbers, such as the Reynolds number, Strouhal number, Weber number, Capillary number, and Ω, in predicting the performance of the inkjet nozzle before introducing the operating conditions.

Keywords

Scaling analysis, Numerical simulation, Inkjet printing, Ultrasonic pulsation atomizer

Cover Page Footnote

This is a fully-reviewed paper expanded from work that was presented at the 9th International Symposium on Scale Modeling (ISSM9), held in March 2022 in Naples, Italy.

Progress in Scale Modeling, an International Journal, Vol. 3, Issue 1 (2022) Article 03-01-03, pp. 1–10
https://doi.org/10.13023/psmij.2022.03-01-03

A CFD-based scaling analysis on liquid and paint droplets moving through a weak concurrent airflow stream

M. Arabghahestani *, N. K. Akafuah, T. X. Li, K. Saito

Institute of Research for Technology Development (IR4TD), University of Kentucky, Lexington, KY 40506, USA

E-mails: masoud.arabghahestani@uky.edu (the corresponding author);
nelson.akafuah@uky.edu (for contact)

Received May 9, 2022, Accepted Jul 28, 2022

Abstract

We conducted volume of fluids (VOF) multiphase model numerical simulations to obtain the interaction among all the major governing forces identified in our previous paper. Our numerical experiments are intended to assess the droplet generation process and the jetting behavior by providing specific input conditions, offering CFD as a tool to study scaling correlations instead of physical experiments. Water droplets that can represent waterborne paints were generated by piezo-generated sinusoidal waveforms at the inlet of the nozzle. The governing forces included the external piezo-based wave-generation force, the inertial force of droplets, the inertial force of air, the viscose force of air acting on droplet surface, the viscous force of liquid, and surface tension force of droplets. The law approach-based scaling theory was applied to explain the significance of traditional pi-numbers, such as the Reynolds number, Strouhal number, Weber number, Capillary number, and Ω, in predicting the performance of the inkjet nozzle before introducing the operating conditions.

Keywords: Scaling analysis; Numerical simulation; Inkjet printing; Ultrasonic pulsation atomizer

Introduction

Fine liquid droplets have a wide range of applications in various fields, including healthcare, automotive, coating, painting, food, combustion, microfluidic devices and pharmaceutical industries [1–10]. Many of these droplets are produced by applying a liquid jet breakup process. Therefore, a complete understanding of the mechanics of liquid breakup to produce fine liquid droplets is crucial for controlling the effective use of these fine droplets. However, the current understanding of the mechanism of liquid breakup and atomization is incomplete, causing a range of unfavorable results and making it difficult for researchers to find the root cause of these problems for improvement by finding an effective cure. These unfavorable results include the generation of satellite drops, variation of droplet sizes, long ligament breakup lengths, droplet bouncing, and liquid jets.

Researchers have searched various factors and concluded that the atomization process is affected by the turbulent behavior of the flow, fluid properties, particle interactions, and, more importantly, the geometrical properties of the device used for the atomization [2, 3, 11–13]. Because of the multiple factor complexity, some researchers turned to simpler atomizer designs and thoroughly studied the control mechanisms [1, 14–17].

Here, we numerically studied the inkjet printing mechanism for the following reasons. The inkjet printing concept has been a subject of study for many researchers since its first introduction in the 1950s. This concept contributed to realizing inkjet printing technology and creating digital images. As the technology has been continuously improved, its broader applications to other fields became possible, including Micro-Electro-Mechanical Systems (MEMS), spray dryers, electronic industries, and coating and painting industries [4, 5, 14, 18–25]. Various attributes associated with this technology, for example, require further studies on the generation mechanism of on-demand droplets and providing more and easier control over the properties of droplets. Such studies include the ultrasonic pulsation atomizer (UPA) [3] and the

Nomenclature

Ca	Capillary number	$U(t)$	Inlet velocity in terms of time
f	Pulsation frequency	U_{max}	Amplitude of sinusoidal inlet velocity
p	Pressure	We	Weber number
R	Nozzle radius	Ω	Omega number
Re	Reynolds number	σ	Surface tension
St	Strouhal number	μ	Viscosity
U	Velocity magnitude	ρ	Density

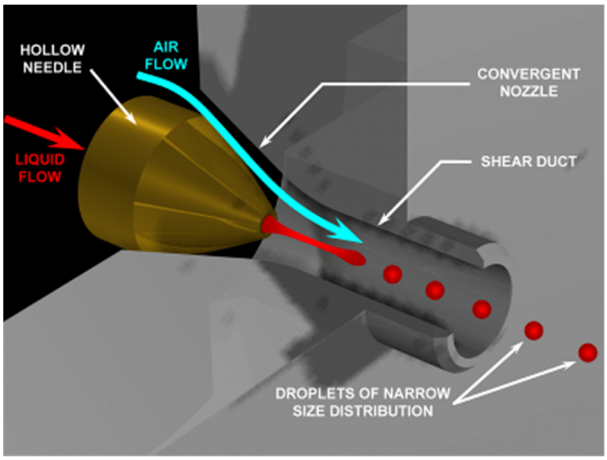

Fig. 1. Isometric view of UPA atomizer used in this study [3, 36, 37]. A continuous liquid flow was provided at the liquid inlet shown on the left hand side with solid red arrow and air was provided through an annular area surrounding the circular nozzle to stabilize the production process of well-regulated droplets coming out from the outlet of the nozzle on the right hand side of UPA. The diameter and length of shear duct attached to the hollow needle can be determined based on the type of liquid, velocity of the droplet and the airflow rate to optimize the steady flow of quality droplet generation at the end.

ultrasonically driven cavitating atomizer (UCA) [14].

Quality control in the generation of droplets demands accurate size droplets without satellite droplets. Castrejon-Pita, et al. studied the factors affecting the liquid breakup and presented the required conditions for the generation of droplets from liquid ligaments using scaling analysis [26]. Eunjeong, et al., Qi, et al., and Fromm all investigated the droplet filaments and the effective factors in controlling their properties using numerical simulations [27–29].

These previous studies helped us understand the control mechanism of inkjet printing technology. The study conducted numerical experiments to test the effect of six different physical forces on the generation of the inkjet droplets described in our previous study and evaluate the role of each of five pi-numbers formed from these six different forces [3]. The traditional experimental approach in scale modeling is to design scale model experiments to validate assumptions based on which scaling laws were developed [30, 31]. Due to the difficulty associated with precision control experiments of inkjet droplet flow dynamics, it would be a great help if we could find a way to use numerical experiments to evaluate the role of identified physical forces in the production of fine liquid droplets. Some previous examples use a combination of scale and numerical modeling: Kuwana, et al. on the steel teeming process, T. Ghosh, et al. on coal mining safety, Nakamura, et al. on micro-diffusion flames, and Kumar, et al. on developing a new device to capture fine coal particles [32–35].

In our study here, we first numerically simulated the performance of the UPA inkjet nozzle and created jetting behavior diagrams to predict the fluid dynamical performance of the droplet generation nozzle based on the properties of the working liquid. Then, we conducted numerical scaling analysis to understand the role of physical forces acting on the inkjet droplet dynamics with the jetting behavior diagrams. A CFD model was developed based on the volume of fluids (VOF) method using ANSYS FLUENT 19.1 commercial software package.

Simulation

The inkjet nozzle used in this study is the UPA nozzle presented in our previous study [3], and an isometric view of that is illustrated in Fig. 1. The nozzle consists of a liquid flow inlet, shaping airflow inlet, liquid injection nozzle, and a shear duct to keep the shear force of the air on the liquid ligament. The liquid velocity is considered to have a sinusoidal waveform, and different wavelengths have been considered to account for the effects of the pulsation frequency on the jetting behavior diagram. However, the air inlet velocity is considered to have constant values in the working range to study the effects of the inertial force of air on the jetting behavior diagram.

Simulation domain

Fig. 2 demonstrates the computational domain designed for this study. The domain includes the inlets, the shear duct and the area between the nozzle and the

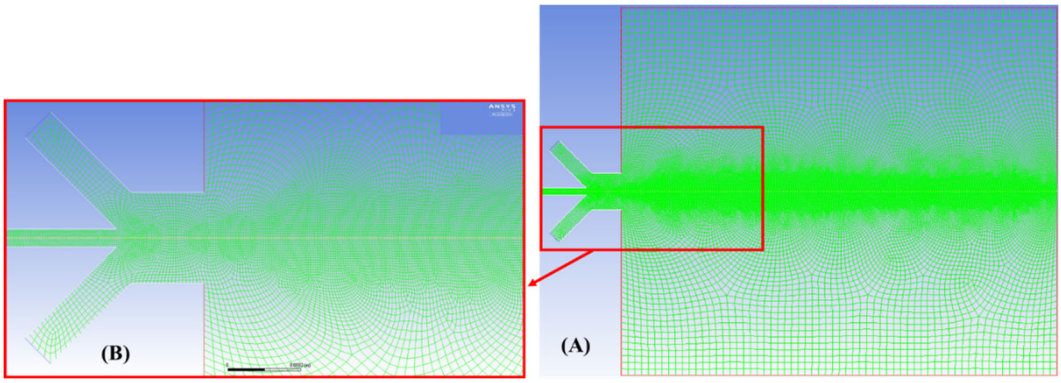

Fig. 2. a) Overall view of the grid generated for the numerical model. b) A detailed figure of the finer mesh near the liquid injection nozzle and along the trajectory of droplets.

targeted substrate to capture the droplets' properties. This domain encompasses the relevant region inside the nozzle and up to 3.2 mm and 1.23 mm outside the nozzle in the axial and radial directions. Volume cells of down to 25 microns were generated to obtain acceptable accuracy of the results. The cell quantity was increased in the areas with higher intensity gradients and mass transfer to capture the physics more accurately. The cell shapes were modified around the edges with sharper angles to capture the gradients better. Multiple computation grids with various cell sizes were generated to ensure the independency of the results from the computation grid. We found that a computational grid with 21,067 cells captured the physics with high accuracy while optimizing the computation time, suitable for this study.

Simulation details

As mentioned before, the liquid inlet velocity was assumed to be in the form of a sinusoidal wave. This is an effective method to reduce the size of the droplets without decreasing the nozzle radius or increasing the shaping air velocity. For the liquid inlet velocity to the nozzle, we proposed Eq. (1), where f represents the pulsation frequency. Both U_{max} and f were changed to study their effects on the atomization process and the droplets' quality.

$$U(t) = |U_{max} Sin(2\Pi f t)| \quad (1)$$

Based on these considerations, the Volume of Fluid (VOF) model available in ANSYS FLUENT software was used to simulate the effects of different factors on the nozzle's performance. No further details are provided here since our previous study offers the numerical simulation method and validation of the code [3].

To simplify the model, the following assumptions were considered.

1. The internal liquid and air flows are laminar.
2. All phenomena are axisymmetric.
3. Airflow is treated incompressible due to low Mach number.
4. The liquid transport properties are constant.
5. Atomization occurs at the standard atmospheric conditions.
6. Evaporation of the liquid ligament and droplets can be neglected for our relatively short droplet dynamics simulation period at the standard room temperature condition. Due to this assumption, the use of the energy equation becomes unnecessary.
7. The computational model was assumed to be 2-D based on assumption 2.

Scaling analysis

After creating the numerical model and successfully simulating fluid dynamics of the droplet formation and transport behavior, we were interested in numerically studying the effects of all significant parameters that influenced this phenomenon. A traditional scale-modeling approach to this task will be a well-designed experiment that can satisfy the accuracy of the numerical simulation and the seven assumptions employed in section "Simulation details" for the numerical model calculations.

This experiment is difficult, so a validated numerical model like the current one can do this task systematically. First, we select a key parameter while keeping the rest of the parameters constant to numerically assess the effects of the key parameter on the fluid dynamics of the generated droplets. Then we change the key parameter and repeat the numerical calculations by following the same procedure for another factor. There were a total of six key parameters (major forces) to be assessed in conjunction with the performance of the inkjet nozzle and the process of breaking up the liquid ligament.

This numerical experiment has merit over scale-model experiments regarding time and consistency. Still, it has limitations associated with assumptions employed for calculations and governing equations that the numerical model uses may not precisely capture the mechanism of the phenomena of concern. Thus, physical experiments, no matter how simple they are, are irreplaceable by numerical models. A direct presentation of nature is only possible by physical experiments,

through which observers may access the secret mystery of nature by their direct observations.

As to the role of experiments, it is noteworthy to mention that S. Poozesh recently addressed the emergence and surge of data-driven modeling as a new opportunity to leverage experimental data in model development, in comparison to the traditional first-principle-based scale modeling, which attempts to find pi-numbers made up of physical forces and energies that govern the phenomenon of concern and proper correlations between pi-numbers [36]. The law approach is available to accomplish the first aim, while scale model experiments achieve the second aim. His mention of data-driven modeling, such as artificial intelligence, can be added as a new tool to scale modeling [38].

These six different forces include: (1) the inertial force of air (F_1), (2) the inertial force of liquid (F_2), (3) viscous force of air acting on droplet surface (F_3), (4) viscous force of liquid (F_4), (5) surface tension force of liquid (F_5), and (6) the dynamic pressure force (flow oscillation force) (F_6) which causes oscillation of liquid flow. Applying the law approach scale modeling theory [38], the following five independent non-dimensional numbers (pi-numbers) can be formed from these six different forces. They are, for example, according to the law approach theory, $\pi_1 = F_1/F_2$, $\pi_2 = F_2/F_3$, $\pi_3 = F_3/F_4$, $\pi_4 = F_4/F_5$, $\pi_5 = F_6/F_5$ and presented in equation (2).

Theoretically, the above five independent pi-numbers (principal pi-numbers) are sufficient to study the performance of the inkjet nozzle. However, the Capillary number, *Ca* defined as the ratio of (v iscous drag force)/(surface tension force) and the Strouhal number, *St*, defined as the ratio of (flow oscillation force)/(inertial force of liquid), can be added as auxiliary pi-numbers, since the viscous drag force in the *Ca* number and the flow oscillation force in the St number are a function of the *Re* number. These two pi-numbers will interest inkjet nozzle design engineers and researchers. The *Ca* number and the *St* number can be respectively described with the principal pi-numbers as follows: $Ca = \pi_3\pi_4$, $St = \pi_5/(\pi_2\pi_3\pi_4)$.

$$\pi_1 = F_1/F_2 = \frac{\text{Inertial force of air}}{\text{Inertial force of liquid}} = \frac{(\rho UR)_{\text{a}}}{(\rho UR)_{\text{l}}}$$

$$\pi_2 = F_2/F_3 = \frac{\text{Inertial force of liquid}}{\text{Viscous force of air}} = \frac{(\rho UR)_{\text{l}}}{(\mu)_{\text{a}}} \quad (2)$$

$$\pi_3 = F_3/F_4 = Re_{\text{l}} = \frac{\text{Inertial force of liquid}}{\text{Viscous force of liquid}} = \frac{(\rho UR)_{\text{l}}}{\mu_{\text{l}}}$$

$$\pi_4 = F_4/F_5 = We_{\text{l}} = \frac{\text{Inertial force of liquid}}{\text{Surface tension force}} = \frac{(\rho U^2 R)_{\text{l}}}{\sigma_{\text{l}}}$$

$$\pi_5 = F_6/F_5 = \Omega^2 = \frac{\text{Flow oscillation force}}{\text{Surface tension force}} = \frac{(f^2\rho R^3)_{\text{a}}}{\sigma_{\text{l}}}$$

$$Ca_{\text{l}} = \frac{\text{Viscous drag force}}{\text{Surface tension force}} = \frac{(\mu U)_{\text{l}}}{\sigma_{\text{l}}} = \pi_4/\pi_3$$

$$St_{\text{l}} = \frac{\text{Flow oscillation force}}{\text{Inertial force of liquid}} = \frac{FR}{U_{\text{l}}} = \pi_5/(\pi_2\pi_3\pi_4)$$

In the above equations, ρ is the density of the liquid/air flow (Kg/m^3), f is the frequency of pulsations (kHz), U is the inlet velocity of the liquid/air flow (m/s) (characteristic velocity chosen in this work), R is the nozzle radius (m) (characteristic length chosen in this work), and σ is the surface tension of the liquid flow (N/m). To test the effectiveness of our numerical experiments, we selected the following two cases: Case 1 dealt with droplet generation with no pulsation, while Case 2 dealt with the liquid flow with pulsation to generate the flow oscillations.

Case 1: The liquid flow without pulsation

With this assumption, the Strouhal and Ω numbers will not affect the numerical calculations, and Case 1 is controlled by five pi-numbers: π_1 through π_4 as principal pi-numbers and the *Ca* number as auxiliary pi-number. We created three different graphs, *Re* (π_3) vs. *Ca*, *We* (π_4) vs. *Ca*, and π_1 vs. π_2, to analyze the effects of the governing forces, the inertial force of air and liquid, the viscous force of air and liquid, and the surface tension force of the liquid.

Fig. 3 presents the jetting behavior diagrams of the nozzle in terms of *Re-Ca*, and Fig. 4 does that in terms of *We-Ca*. These two graphs separate the conditions with which the nozzle could produce monodispersed droplet stream. The blue dots represent the tests with monodispersed droplet streams, while the orange dots represent cases with satellite droplets or long liquid ligaments/spray; this process was repeated for all other graphs presented in this work. To plot these two graphs, the air velocity, surface tension, liquid, air densities, and the geometric properties of the nozzle were assumed to be constant. To obtain a sufficient number of data to establish a clear trend, the liquid inlet velocity was changed from 0.25 m/s to 5 m/s, and the viscosity was changed from μ_w up to $10\mu_w$. Note that the air velocity chosen for these tests was 10m/s due to its optimum value to produce droplets from the working

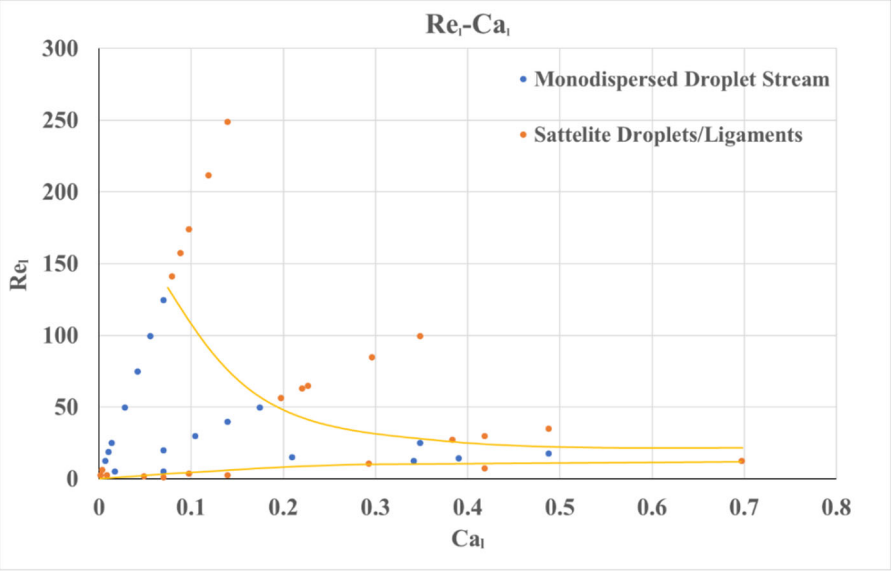

Fig. 3. Jetting behavior diagram separating the regions with monodispersed droplet stream and satellite droplets droplet generation/ligament in terms of *Re* and *Ca* numbers.

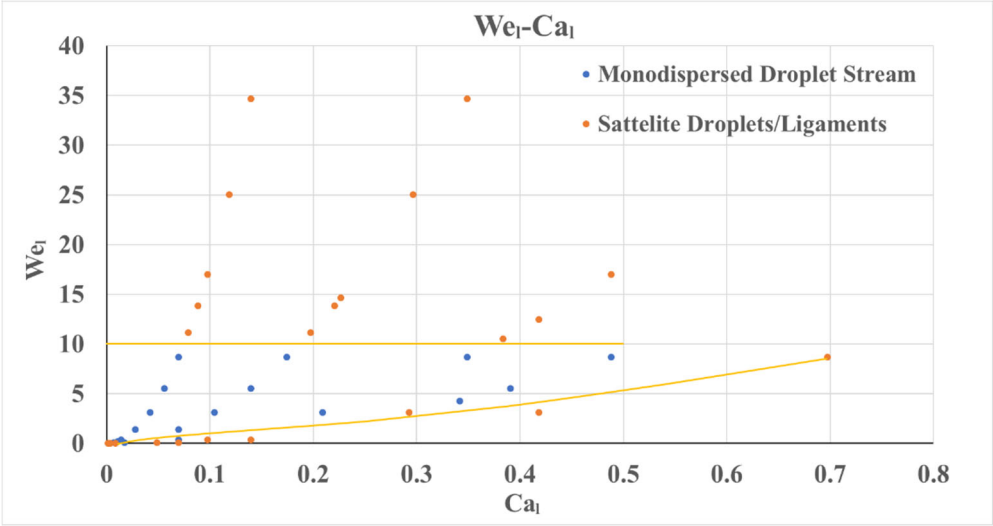

Fig. 4. Jetting behavior diagram separating the regions with monodispersed droplet stream and satellite droplets droplet generation/ligament in terms of *We* and *Ca* numbers.

liquid of the desired diameter, even under an increasing liquid viscosity.

Figs. 3 and 4 show that three principal pi-numbers govern the jetting process without oscillation and air inertial forces. As shown from the data in Fig. 3, there is a maximum *Re* number for each *Ca* number with which condition the nozzle can generate a stream of monodispersed droplets. For example, suppose the viscous force is kept constant while increasing the *Re* number by increasing the inertial force of the liquid. In that case, the surface tension force of the working fluid needs to be changed not to produce satellite droplets. An increase in the *Ca* number decreases the maximum *Re* number, a maximum inertial force at which the breakup occurs.

Fig. 3 shows that the *Ca* number has less influence on the atomization process in higher *Re* number regions. Note that the range for which the nozzle can generate monodispersed droplet streams in higher *Ca* numbers is very narrow since the nozzle's performance decreases significantly for working liquids with higher viscosity. Fig. 4 presents this information with a different scale. The *Re-Ca* graph can also be shown in a *We-Ca* graph since the surface tension was assumed to be constant.

Shaping air influences the quality of droplets [39]; therefore, we focused on observing its effects for determining the ideal air velocity that can produce monodispersed droplet stream. The following section assesses the impact of shaping air velocity on the atomization process with two principal pi-numbers, π_1 and π_2, which count on the effects of the inertial force of the

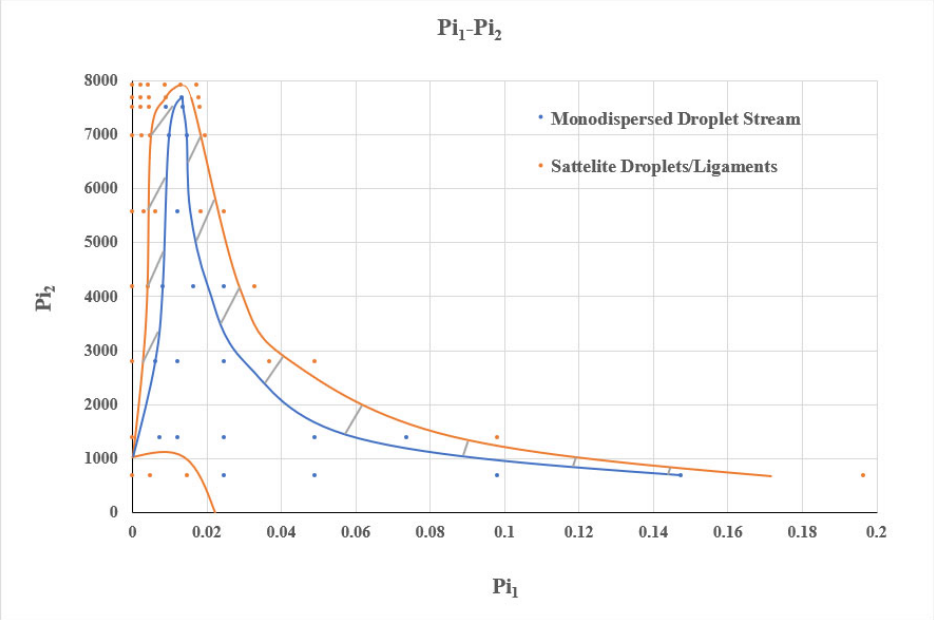

Fig. 5. Jetting behavior diagram separating the regions with monodispersed droplet stream and satellite droplets droplet generation/ligament in terms of Pi_1 and Pi_2 numbers.

Table 1. Droplet diameters for some of the tests presented in Fig. 3 to Fig. 5 with no pulsation and viscosity of μ_w.

Re_l	Re_a	Pi_1	Pi_2	We_l	Oh_l	Ca_l	Droplet Diameter
24.88	248.8	0.049	1394.6	0.35	0.02	0.01	70 µm
74.64	248.8	0.016	4183.8	3.12	0.02	0.04	76 µm
74.64	124.4	0.008	4183.8	3.12	0.02	0.04	74 µm
74.64	373.2	0.025	4183.8	3.12	0.02	0.04	65 µm

liquid, the inertial force of the air, and the viscous force of the air.

Fig. 5 presents the jetting behavior diagrams of the nozzle in terms of the two pi-numbers, π_1 and π_2. The liquid inlet velocity was changed from 0.5 m/s to 5.67 m/s, and the air velocity was changed from 0 to 20 m/s to study its effects on the atomization process, while the air and liquid viscosities, surface tension, and air and liquid densities were kept constant. As shown in Fig. 5, the nozzle cannot produce quality droplets without having shaping air ($\pi_1 = 0$).

Fig. 5, unlike *Re-Ca* and *We-Ca* graphs, shows a transition area boundary between the two regions as a solid line due to uncertainties in the atomization process and the numerical assumptions or simply due to the hardship of separating the quality of the droplets qualitatively. Fig. 5 shows that for each specific π_2 number, there was a minimum and a maximum shaping air velocity to control the atomization process and ensure the generation of monodispersed drops. The minimum air velocity increases with an increase in the inertial force of the liquid. In contrast, the change in the maximum air velocity is much more significant, as shown in Fig. 5. For higher liquid inertial forces, the production of quality droplets becomes less influenced by the shaping air, and the average shaping air velocity required to produce quality droplets is lower. There may be a minimum liquid inertial force to generate a droplet stream due to the nozzle surface's wettability effects.

Now that we observed the behavior of the droplets and the nozzle's performance with different dimensionless numbers, it is worthy to briefly analyze how this changes the average diameter of the droplets as well since this factor is important for various applications of inkjet nozzles and could be helpful to understand the mechanisms behind this process. The trend of droplet diameter could be more easily observed by analyzing the nozzle's performance for each different influential parameter as it is provided in our previous work [3], but it is still helpful to provide some of the data to have a better understanding of the droplet diameter change with these dimensionless numbers. Table 1 shows the droplet diameters for some of the tests presented in Fig. 3 to Fig. 5. Note that Table 1 focuses on providing the droplets diameters only for the cases that the nozzle produced a complete stream of

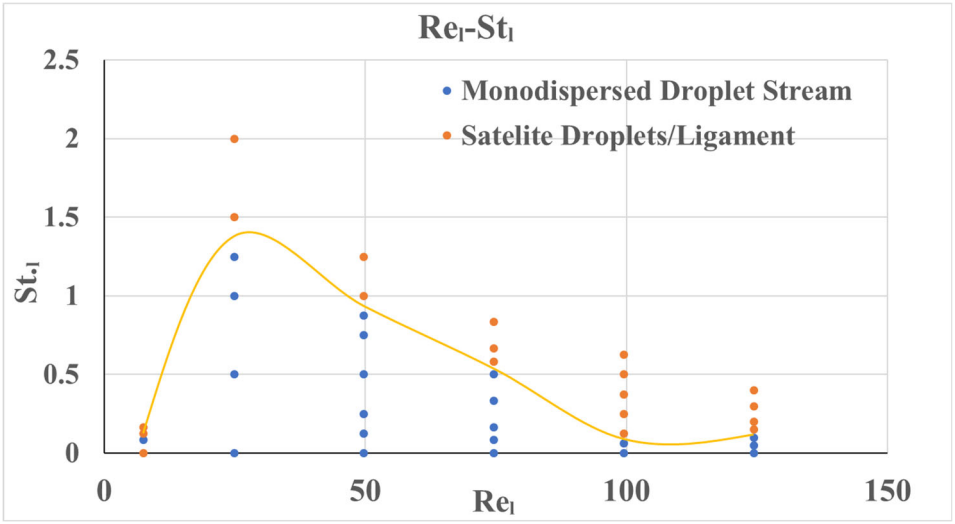

Fig. 6. Jetting behavior diagram separating the regions with monodispersed droplet stream and satellite droplets droplet generation/ligament in terms of *Re* and *St* numbers.

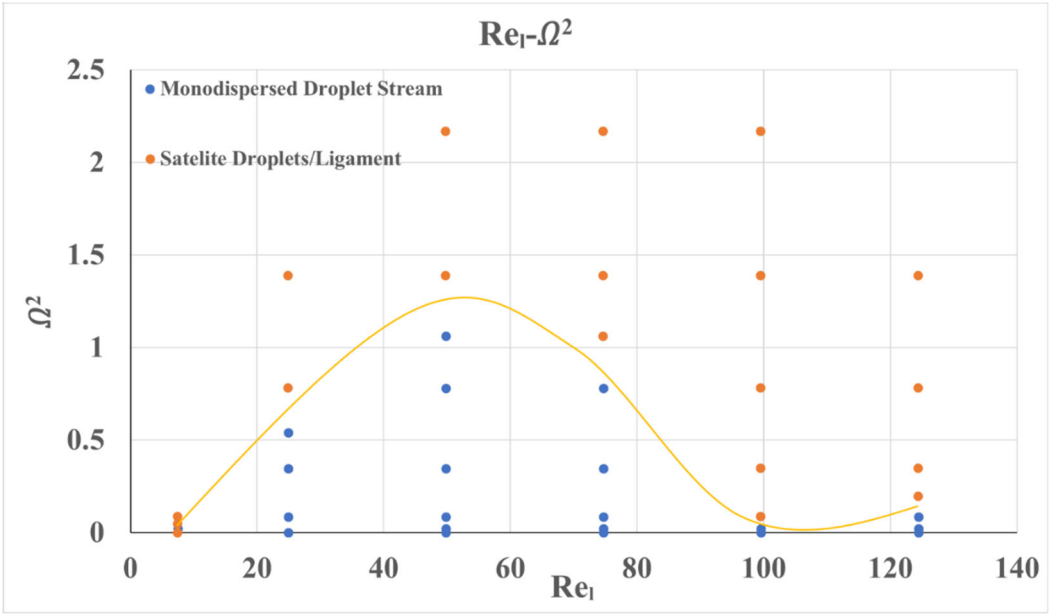

Fig. 7. Jetting behavior diagram separating the regions with monodispersed droplet stream and satellite droplets droplet generation/ligament in terms of *Re* and Ω^2 numbers.

monodispersed droplets. As it can be observed from the data in this table, *Re*, π_1, π_2 and *We* numbers does not affect the droplet sizes significantly if the pulsation frequency and liquid viscosity are assumed to be constant as the maximum change was less than 17%. This percentage will be presented, for when the liquid viscosity and pulsation were changed, later in this work.

Note that, in all the cases provided in this table, the liquid viscosity was assumed to be μ_w and the data for higher viscosity fluids will be presented later to compare those with those of pulsating flow.

Case 2: The liquid flow with pulsation

This case includes the form of sinusoidal waves in liquid inlet velocity and studies the effects of the pulsation frequency on the droplet generation. Fig. 6 shows *Re* (π_3) vs. *St*. The interactions among the inertial force of liquid, viscous force of liquid, and flow oscillation force was calculated by keeping all other forces constant. Fig. 7 shows *Re* vs. Ω^2 (π_5), where the interactions of the inertial force of liquid, the viscous force of liquid, surface tension force, and flow oscillation force was calculated by keeping all other forces constant.

Figs. 6 and 7 present the jetting behavior diagrams of the nozzle under the conditions that the air velocity, surface tension, liquid and air densities, and the geometric properties of the nozzle are constant, while the liquid inlet velocity was changed from 1 m/s to 5 m/s

Table 2. Droplet diameters for some of the tests with higher viscosity fluids.

Re_l	We_l	Oh_l	Ca_l	Omega	Droplet Diameter
14.93	3.12	0.12	0.21	0	81 µm
29.86	3.12	0.06	0.1	0	65 µm
74.64	3.12	0.02	0.04	0	76 µm
10.66	3.12	0.17	0.29	0.15	57 µm
14.93	3.12	0.12	0.21	0.22	55 µm
74.64	3.12	0.02	0.04	0.15	48 µm
74.64	3.12	0.02	0.04	0.29	52 µm
74.64	3.12	0.02	0.04	0.59	62 µm
74.64	3.12	0.02	0.04	0.88	69 µm

and the liquid viscosity from μ_w up to $10\mu_w$.

Fig. 6 shows that there is a maximum *St* number for each *Re* number for which the generation of uniform droplet stream is possible. The maximum frequency is relatively low for high *Re* numbers, while it increases with a decrease in the *Re* number. This data is useful to generate smaller droplets with relatively low liquid droplet speeds (i.e., low inertial forces of liquid). For very low Reynolds numbers, e.g. Reynolds numbers lower than 10 (e.g., high viscosity working liquids, such as industry paints), the range of frequencies that can be used is minimal as it can be seen for lower *Re* numbers in both Figs. 6 and 7. This confirmed that generating droplets using higher viscosity working liquid was more challenging and required specific frequencies. Note that generation of monodispersed droplet stream was possible without frequency in most cases except when the viscosity was very high ($7\mu_w$), for which there was a minimum frequency (10KHz) required. Fig. 7 shows this information in terms of *Re* and Ω^2. The data in the two graphs of Figs. 6 and 7 can easily be converted to each other since the surface tension was assumed to be constant in all cases.

Now we can look at the changes in droplet diameter with respect to these dimensionless numbers again to have an understanding of the trend. Again, the trend of droplet diameter could be more easily observed by analyzing the nozzle's performance for each different influential parameter as it is provided in [3], but it is still helpful to provide some of the data to have a better understanding of the droplet diameter change with these dimensionless numbers. Table 2 presents the droplet diameters for some of the tests presented in this paper with a focus on the effects of omega number and mainly to understand these effects for higher viscosity working fluids. The maximum percentage of change in droplet diameter for the data presented in Table 2, was about 69%, which is much higher than the same percentage for the data presented in Table 1. This shows the significant effects of liquid viscosity and pulsation frequency on droplet diameters generated from the nozzle. By analyzing the data in this table further and comparing the data in the 3rd and 6th rows in this table, we notice about 58% difference in droplet diameter by only introducing pulsation frequency as the only dimensionless number that is different is Omega. This emphasizes on the importance of pulsation frequency (with the right wave form) in reducing the droplet size without reducing the nozzle's radius. This is very important as many industry applications require smaller droplets but reducing the nozzle's radius can have negative effects such as nozzle clogging, depending on the application.

Note that Table 2 focuses on providing the droplets diameters only for the cases that the nozzle produced a complete stream of monodispersed droplets.

Conclusions

Conclusions from this study are summarized as follows.

(1) We conducted CFD modeling to assess the performance of the UPA inkjet atomizer under various working conditions working with waterborne (WB) paints as the working liquid. The aims of this study are to understand the effects of the effective parameter on the nozzle's performance, especially using higher viscosity WB paints as the working liquid. This will help improve the nozzle's performance and provide precision control over the quality of the generated droplets, improving the transfer efficiency of the atomization process and reducing material waste.

(2) We conducted scaling analysis to analyze the correlations between single monodispersed droplet stream and satellite droplet jetting conditions and provide jetting behavior diagrams to predict the performance of the inkjet nozzles under different

conditions. Our scaling analysis showed that there are six influential forces responsible for controlling the quality of the droplets and the performance of the process, eventually forming five independent pi-numbers. These six forces are the inertial force of air, the inertial force of liquid, viscous force of air acting on droplet surface, the viscous force of liquid, surface tension force of liquid, and dynamic pressure force (flow oscillation force).

(3) We showed how to analyze the interactions among all these six independent governing forces and generate a very narrow and monodispersed droplet stream from the nozzle for each condition.

(4) Finally, we obtained the jetting behavior diagram of the UPA nozzle for different conditions by identifying five independent pi-numbers (principal pi-numbers) with significant effects on the nozzle's performance. This diagram can significantly help engineers and researchers to efficiently and effectively design their desired inkjet nozzles that can satisfy their aims.

Acknowledgments

This study was supported by the Institute of Research for Technology Development (IR4TD) research enhancement fund at the University of Kentucky.

References

[1] Liu, H., Science and Engineering of Droplets: Fundamentals and Applications, William Andrew, 2002.

[2] Lefebvre, A. H., Atomization and Sprays, Hemisphere Pub., 1989.

[3] Arabghahestani, M., Akafuah, N. K., Saito, K., "Computational fluid dynamics and scaling study on ultrasonic pulsation atomizer for waterborne paint," Atomization and Sprays 31(3): 29–52,2021.

[4] Basaran, O. A., "Small-scale free surface flows with breakup: drop formation and emerging applications," AIChE Journal 48(9): 1842–1848, 2002.

[5] Arabghahestani, M., Poozesh, S., Akafuah, N. K., "Advances in computational fluid mechanics in cellular flow manipulation: a review," Applied Sciences 9(19): 4041, 2019.

[6] Arabghahestani, M., Karimian, S. M. H., "Molecular dynamics simulation of rotating carbon nanotube in uniform liquid argon flow," Journal of Molecular Liquids 225: 357–364, 2017.

[7] Li, H., Pokhrel, S., Schowalter, M., Rosenauer, A., Kiefer, J., Mädler, L., "The gas-phase formation of tin dioxide nanoparticles in single droplet combustion and flame spray pyrolysis," Combustion and flame 215: 389–400, 2020.

[8] Gao, J., Hossain, A., Matsuoka, T., Nakamura, Y., "A numerical study on heat-recirculation assisted combustion for small scale jet diffusion flames at near-extinction condition," Combustion and flame 178: 182–194, 2017.

[9] Babaei, A., Arabghahestani, M., "Free vibration analysis of rotating beams based on the modified couple stress theory and coupled displacement field," Applied Mechanics 2(2): 226–238, 2021.

[10] Hossein K. S. M., Hasheminasab, S. M., Arabghanestany, M., "Molecular dynamics simulation of stationary and rotating nanotube in uniform liquid argon flow," 4th Micro and Nano Flows Conference, UCL, London, UK, Sept. 7–10, 2014.

[11] Nasr, G. G., Yule, A. J., Bendig, L., Industrial Sprays and Atomization: Design, Analysis and Applications, Springer Science & Business Media, 2013.

[12] Bergwerk, W. "Flow pattern in diesel nozzle spray holes," Proceedings of the Institution of Mechanical Engineers 173(1): 655–660, 1959.

[13] Dong, H., Carr, W. W., Morris, J., "An experimental study of drop-on-demand drop formation," Physics of fluids 18(7): 072102, 2006.

[14] Akafuah, N. K., Salazar, A. J., Saito, K., Srinivasan, V., "Ultrasonically driven cavitating atomizer: prototype fabrication and characterization," ASME 2009 Fluids Engineering Division Summer Meeting, 2009.

[15] Avvaru, B., Patil, M. N., Gogate, P. R., Pandit, A. B., "Ultrasonic atomization: effect of liquid phase properties," Ultrasonics 44(2): 146–158, 2006.

[16] Janna, W. S., Drop-size Distributions of Sprays Produced by Fan-jet Pressure Nozzles, PhD Thesis, University of Toledo, Toledo, USA, 1976.

[17] Darwish Ahmad, A., Singh, B. B., Doerre, M., Abubaker, A. M., Arabghahestani, M., Salaimeh, A. A., Akafuah, N. K., "Spatial positioning and operating parameters of a rotary bell sprayer: 3D mapping of droplet size distributions," Fluids 4(3): 165, 2019.

[18] Abu-Khalaf, J., Al-Ghussain, L., Nadi, A., Saraireh, R., Rabayah, A., Altarazi, S., Al-Halhouli, A., "Optimization of geometry parameters of inkjet-printed silver nanoparticle traces on PDMS substrates using response surface methodology," Materials 12(20): 3329, 2019.

[19] Antonopoulou, E., Harlen, O. G., Walkley, M. A., Kapur, N., "Jetting behavior in drop-on-demand printing: laboratory experiments and numerical simulations," Physical Review Fluids 5(4): 043603, 2020.

[20] Bernardini, G. L., Rampy, B. A., Howell, G. A., Hayes, D. J., Frederickson, C. J., "Applications of piezoelectric fluid jetting devices to neuroscience research," Journal of Neuroscience Methods 38(1): 81–88, 1991.

[21] Castrejón-Pita, A. A., Castrejón-Pita, J. R., Martin, G. D., "A novel method to produce small droplets from large nozzles," Review of Scientific Instruments 83(11): 115105, 2012.

[22] Hutchings, I. M., Martin, G. D., Inkjet Technology for Digital Fabrication, John Wiley & Sons, 2012.

[23] Wijshoff, H., "The dynamics of the piezo inkjet printhead operation," Physics Reports 491(4–5): 77–177, 2010.
[24] Poozesh, S., Akafuah, N., Saito, K., "Numerical simulation of a coating sprayer capable of producing controllable paint droplets," SAE Technical Paper, 2015.
[25] Burr, R. F., Tence, D. A., Le, H. P., Adams, R. L., Mutton, J. C., "Method and apparatus for producing dot size modulated ink jet printing," U.S. Patent No. 5,495,270, 1996.
[26] Castrejon-Pita, A. A., Castrejon-Pita, J. R., Hutchings, I. M., "Breakup of liquid filaments," Physical Review Letters, 108(7): 074506, 2012.
[27] Kim, E., Baek, J., "Numerical study on the effects of non-dimensional parameters on drop-on-demand droplet formation dynamics and printability range in the up-scaled model," Physics of Fluids 24(8): 082103, 2012.
[28] Xu, Q., Basaran, O. A., "Computational analysis of drop-on-demand drop formation," Physics of Fluids 19(10): 102111, 2007.
[29] Fromm, J., "A numerical study of drop-on-demand ink jets," in: Le Croissette, D. H. (Ed.), Proceedings of the 2nd International Colloquium on Drops and Bubbles, 1982, pp. 54–62.
[30] Saito, K., Progress in Scale Modeling: Summary of the First International Symposium on Scale Modeling (ISSM I in 1988) and Selected Papers from Subsequent Symposia (ISSM II in 1997 through ISSM V in 2006), Springer Science & Business Media, 2008.
[31] Saito, K., Williams, F. A., "Scale modeling in the age of high-speed computation," in: Saito, K. et al. (Eds.), Progress in Scale Modeling, Volume II, Springer, 2015, pp. 1–18.
[32] Kuwana, K, Hassan, M. I., Singh, P. K., Saito, K., Nakagawa, J., "Scale-model experiment and numerical simulation of a steel teeming process," Materials and Manufacturing Processes 23(4): 407–412, 2008.
[33] Ghosh, T., Rezaee, M., Honaker, R. Q., Saito, K., "Scale and numerical modeling of an air-based density separator," in: Saito, K. et al. (Eds.), Progress in Scale Modeling, Volume II, Springer, 2015, pp. 225–238.
[34] Nakamura, Y., Yamashita, H., Saito, K., "A numerical study on extinction behaviour of laminar microdiffusion flames," Combustion Theory and Modelling 16(6): 927–938, 2006.
[35] Kumar, A. R., Arya, S., Levy, A., Schafrik, S., Wedding, W. C., Saito, K., "Scale and numerical modeling to determine operating points of a non-clogging Vortecone filter in mining operation," Progress in Scale Modeling, an International Journal, 1(1): 7, 2020.
[36] Poozesh, S., "Data-driven tools guided by first-principles for scale modeling," Progress in Scale Modeling, an International Journal, 2(1): 1, 2021.
[37] Arabghahestani, M., Akafuah, N. K., Li, T. X., Saito, K., "A Cfd-based scaling analysis on liquid droplets moving through a weak concurrent airflow stream," International Symposium on Scale Modeling, Napoli, Italy, Mar. 2–4, 2022.
[38] Emori, R. I., Saito, K., Sekimoto, K., Scale Models in Engineering (Mokei Jikken no Riron to Ohyou), Gihodo Publishing Co., Tokyo, Japan, 2000.
[39] Toda, K., Salazar, A., Saito, K., Automotive Painting Technology: A Monozukuri-Hitozukuri Perspective, Springer, 2012.